Numerical and Experimental study of aircraft engine ignition

G. Linassier*, R. Lecourt, P. Villedieu, G. Lavergne, H. Verdier†
* ONERA, Département Modèles pour l'aérodynamique et l'énergétique,
BP 4025, 31055 Toulouse Cedex, France
† TURBOMECA, 64511 Bordes Cedex, France

Abstract

The aim of this study is to develop and validate an ignition model, which could be coupled with a CFD code to predict ignition/re-ignition of an aircraft engine. This model is validated using a data base acquired on the MERCATO test rig (ONERA/Fauga-Mauzac), reproducing a simplified combustion chamber. A simulation of the two-phase flow inside the chamber has been performed and compared with experimental data for a non-reactive flow, just before ignition. The spray ignition model has been tested for several positions of the spark plug device.

Introduction

With the reduction of pollutant emissions level, industrials must design novating combustion chamber, allowing lean combustion. In the case of relight at high altitude, corresponding to critical conditions, ignition can't be correctly predicted by current methods used in industry. A parametric experimental study on a real combustion chamber is very expensive, and cannot be used to test all possible geometries during development process. CFD remains the cheaper solution, although modelling of the spray ignition is rather complex. Moreover, the complete modelling of spark discharge recquires great computational cost, to take into account plasma effects or detailed chemistry schemes.

In the litterature, there are few studies about two-phase flow combustion for industrial configurations. Widmann [1] worked on a methanol spray in a swirled air flow, characterizing the droplet velocity with and without combustion. Ikeda et al [2] studied the influence of pressure on a burning diesel spray in a highly-pressurized swirl-stabilized combustor. Hochgreb et al [3] studied relight at high-altitude conditions for a lean combustor. With high speed imaging, they tracked the motion and break-up of the flame during the propagation phase. Recently, Mastorakos et al [4] studied the ignition of a n-heptane spray with multiple sparks. Using a mobile spark plug device, they established a map of ignition probability into a closed vessel, and identified parameters optimizing ignition.

Through three thesis, ONERA developed a simplified spray ignition model. This model can be coupled with a RANS code to simulate ignition of a combustion chamber by a spark plug. Quintilla[5] has developed a 0D ignition model, allowing to compute the temperature evolution of the ignition kernel. Ouarti[6] used this model to perform a 2D axisymmetric RANS simulation of several ignition cases. Although these simplifications, ignition tendencies were well reproduced, and the model allowed to discriminate successful ignition cases. Recently, García-Rosa[7] developed an 1D ignition model, which computes the growth of the ignition kernel. This model has been partially validated for gaseous, monodisperse and polydisperse two phase mixtures[8].

In the present work, the 1D ignition model is tested with the results of a 3D simulation of a two-phase flow on the MERCATO test rig. Non-reactive simulations are performed using the CFD code CEDRE (ONERA), with RANS method for the air flow and Lagrangian stationnary approach for the liquid flow. Results are validated with LDA (Laser Doppler Anemometry) and PDI (Phase Doppler Interferometry) measurements.

For the liquid phase, stationnary approach allow to carry out fast simulations, but cannot be used to perform a complete ignition simulation of a chamber, because of the unsteady nature of the phenomena. Until now, we limit our study to the early formation of the ignition kernel. The kernel transport is out of the scope of our work.

Spray kernel ignition model

The aim of the present model is to simulate the early propagation of an ignition kernel in a two-phase mixture. The energy deposition is considered as an instantaneous, adiabatic and isobaric heating process, which creates a spherical flame. The expansion or extinction of this kernel depends on the local equivalence ratio. With these hypothesis, the kernel growth phase is described by numerical resolution of conservation equations for 1D dilute-spray mixture (*See* Eqs. 1, 2 and 3).

*Corresponding author: guillaume.linassier@onera.fr

The computational domain is depicted by Fig. 1. The energy deposite takes place in a spherical volume of radius r_0, at temperature T_∞. This volume expands to a radius $r_1 > r_0$ and temperature rises to T_1. Initial conditions r_1 and T_1 are estimated using kernel vizualisation and knowing the energy of the spark discharge.

$$\frac{\partial \rho_g}{\partial t} + \frac{1}{r^2}\frac{\partial}{\partial r}\left(r^2 \rho_g \, u_{r,g}\right) = \dot{\rho}_{l,v} \tag{1}$$

$$\rho_g \frac{\partial Y_i}{\partial t} + \rho_g \, u_{r,g} \frac{\partial Y_i}{\partial r} - \frac{1}{r^2}\frac{\partial}{\partial r}\left(r^2 \rho_g \mathcal{D}_{i,g} \frac{\partial Y_i}{\partial r}\right) = \dot{\rho}_{l,v}(\delta_{i,\mathrm{F}} - Y_i) + \dot{\rho}_{i,\chi} \tag{2}$$

$$\rho_g c_{p_g} \frac{\partial T_g}{\partial t} + \rho_g \, u_{r,g} \frac{\partial h_g}{\partial r} - \frac{1}{r^2}\frac{\partial}{\partial r}\left(r^2 \lambda_g \frac{\partial T_g}{\partial r}\right) = \dot{\mathcal{H}}_v - \dot{\rho}_{l,v} h_{l,(g)} + \dot{\mathcal{H}}_\chi \tag{3}$$

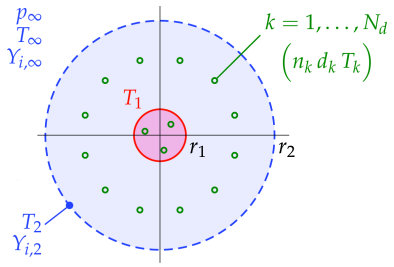

Figure 1. Computational domain for modelization of ignition kernel growth

Kerosene is represented by pure n-decane, and by a polydiperse mixture of N_d diameter classes. The particle distribution function is assumed to be a log-normal one, defined by D_{10} and D_{32}. The liquid equivalence ratio Φ_l is defined as :

$$\Phi_l = \frac{\bar{\rho}_l}{\rho_{g,\infty} \cdot \alpha_s} \tag{4}$$

with $\bar{\rho}_l$ the partial liquid density of kerosene, α_s the stoechiometric Fuel-Air-Ratio, and $\rho_{g,\infty}$ the air density far from the computational domain. Combustion of n-decane is modeled by a one-step chemical reaction with an Arrhenius-type reaction rate $\dot{\omega}$ proposed by Westbrook and Dryer [9] :

$$\mathtt{C_{10}H_{22}} + \left(\frac{31}{2}\right)\mathtt{O_2} \xrightarrow{\dot{\omega}} 10\,\mathtt{CO_2} + 11\,\mathtt{H_2O}. \tag{5}$$

For a complete description of the model, *See* [7]. The model had been used to carry several parametrical studies to test the influence of the equivalence ratio, for gaseous, monodiperse and polydisperse mixtures [8]. The evolution of the flame speed S_L is correctly restitued for gaseous mixture. For monodisperse mixture, our study showed that the minimum ignition delay time increases with the diameter. Finally, ignition of several polydisperse cases had been compared to results of monodisperse cases, to find an equivalent diameter.

Experimental study

The MERCATO test rig allows to reproduce the operating conditions of a combustion chamber in high altitude (low pressure, low temperature). It is equiped with a square-section combustion chamber of 130x130x250 mm^3, with optical access on the front and lateral sides (*See* Fig. 2). The injection system is designed by Turbomeca, and is composed of a pressure atomizer and an air swirler. The ignition device is a spark plug, triggered at 6Hz, which can be mounted on one of the lateral windows.

When using optical measurement with liquid-gas flow in a confined environment, one of the major issue is to deal with the streaming of the liquid on the windows, which possibly degrades measurement quality. It is particularly true at ambiant temperature, but with high temperature, streaming can be minimized. Since, two

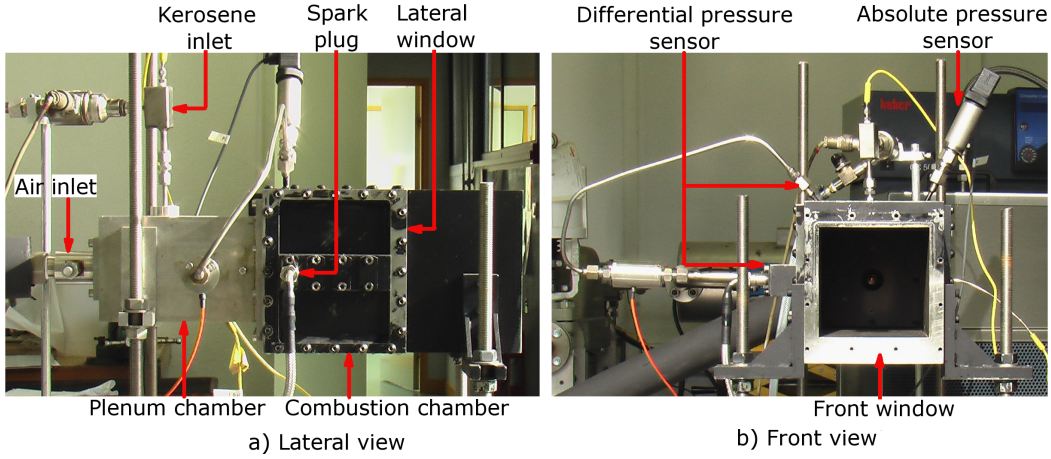

Figure 2. MERCATO combustion chamber.

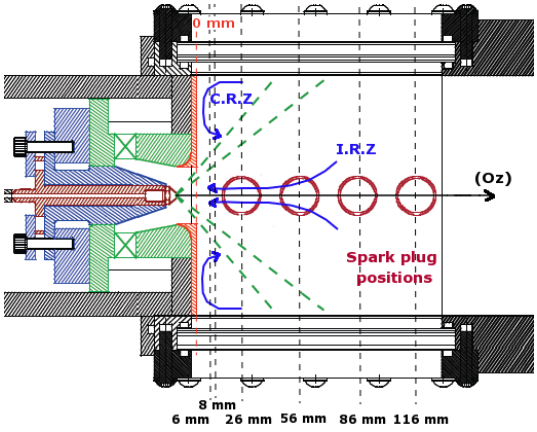

Figure 3. MERCATO diagram; identification of C.R.Z, I.R.Z, spark plug, measurements plane and injector axis.

operating points (OP) have been choosen :

OP1 : T = 463 K ; P_a ; $\dot{m}_g = 35.00 \cdot 10^{-3} kg/s$; $\dot{m}_l = 1.00 \cdot 10^{-3} kg/s$

OP2 : T = 293 K ; P_a ; $\dot{m}_g = 19.38 \cdot 10^{-3} kg/s$; $\dot{m}_l = 2.25 \cdot 10^{-3} kg/s$

To validate our CFD simulations, we define the following strategy :

1. validation of the two phase flow simulation field for OP1, using LDA and PDI data,
2. simulation of OP2 using the same methodology, and test of the ignition model.

All given locations (spark plug, measurement...) are relative to the bottom wall of the chamber (*See* Fig. 3). The possible spark plug positions are {26;56;86;116} mm. *See* Tab. 1 for a synthesis of the available experimental results.

Ignition kernel growth

To simulate spray ignition, we need to estimate the initial size of the kernel. For this purpose, we used a high-speed Video Camera Phantom v9.1 to capture the very early formation of the kernel. The acquisition rate is set at 50 kHz, and the resolution is 96x96 pixels. In our previous study, vizualisation were realized for a spark without fuel. For the present work, we analysed pictures for successful ignition tests, and used a constant threshold level to estimate a mean size of the kernel on several recording.

We obtained vizualisations from lateral and front side of the chamber. The kernel appears as a disk on the lateral view, and as an ellipse on the front view just at the beginning of the recording (*See* Fig. 4). Considering the

Table 1. Experimental data base for the two operating points (x : available ; o : not available; for LDA or PDI, localization of the measurement plane)

	PDI	LDA	Ignition tests	Kernel imaging
O.P 1	6-26-56 mm	8-26-56-86-116 mm	o	o
O.P 2	6 mm	o	x	x

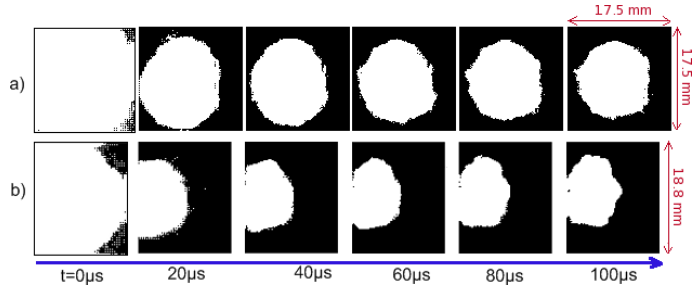

Figure 4. Kernel vizualisation, (a: lateral view; b: front view).

kernel as a spheroid, we estimated his volume as $844mm^3$. The radius of a sphere with same volume would be 5.86 mm.

We observe that the kernel is quickly carried by the flow. Because of our hypothesis of the expansion of a motionless kernel, we must be careful with our ignition simulation duration. We estimated that the kernel moves a distance equal to his diameter around 0.4 ms after the spark discharge occured. Complementary work is to be done to catch the expansion or extinction of the kernel.

LDA characterization of the air flow

For LDA and PDI measurements, we use a two laser-probe device 200-MD from Artium. Assuming the cylindrical symmetry of the air flow, we measure the complete 3D gas velocity field for a plane orthogonal to the axis of the injector nozzle with two crossings,one horizontal (couple of component $u_{z,g}/u_{\theta,g}$) and one vertical ($u_{z,g}/u_{r,g}$). We measure mean and RMS value for each component. Measurements have been carried out for OP1, in the sections located at {8;26;56;86;116} mm. Complete results had been released in [13].

PDI characterization of the liquid flow

PDI was used to measure size and velocity of kerosene droplets. The procedure adopted is the same than with LDA. For OP1, measurements are available for planes {6;26;56} mm, whereas for OP2, the kerosene flow field has been characterized only at 6 mm. Due to the atomization process and the limitation of the aperture angle of the laser beams, we cannot approach closer to the injector nozzle than this position.

Initial conditions for liquid-flow simulation

We use a coincidence filter, which enables to measure simultaneously two velocity components for each particle. Then we calculate the mean velocity components for several diameter classes of particles, and use these classes for our simulation. The same approach has been adopted by Chrigui et al [12]. We noticed that some of the velocity histogramms were multi-gaussian shaped, essentially in the peripherical zone of the spray (*See* Fig. 5). This tendency is explained by local recirculations of the smallest particles, in center and peripherical zones of the spray. The velocity of the particles trapped in recirculation is lower than for particles coming directly from the injector.

At 6 mm, we applied a mixture modelling approach, using a software developped by Biernacki et al[10], interfaced with MATLAB. For each measurement point, we modeled the particle distribution function among the two velocity components as a 2D gaussian mixture. Each gaussian is identified as a cluster of particles, and we can calculate the mean velocity components and diameters. We confirmed the existence of clusters with low diameter

and low velocity, and identified them as a consequence of the recirculation structures. We estimated the kerosene recirculation flow rate around 10% of the total liquid flow rate, which is not negligible. To define our injection parameters for CFD, on the 6 mm plane, these particles have been eliminated, as simulation restitutes recirculating structures (*See* Fig. 6).

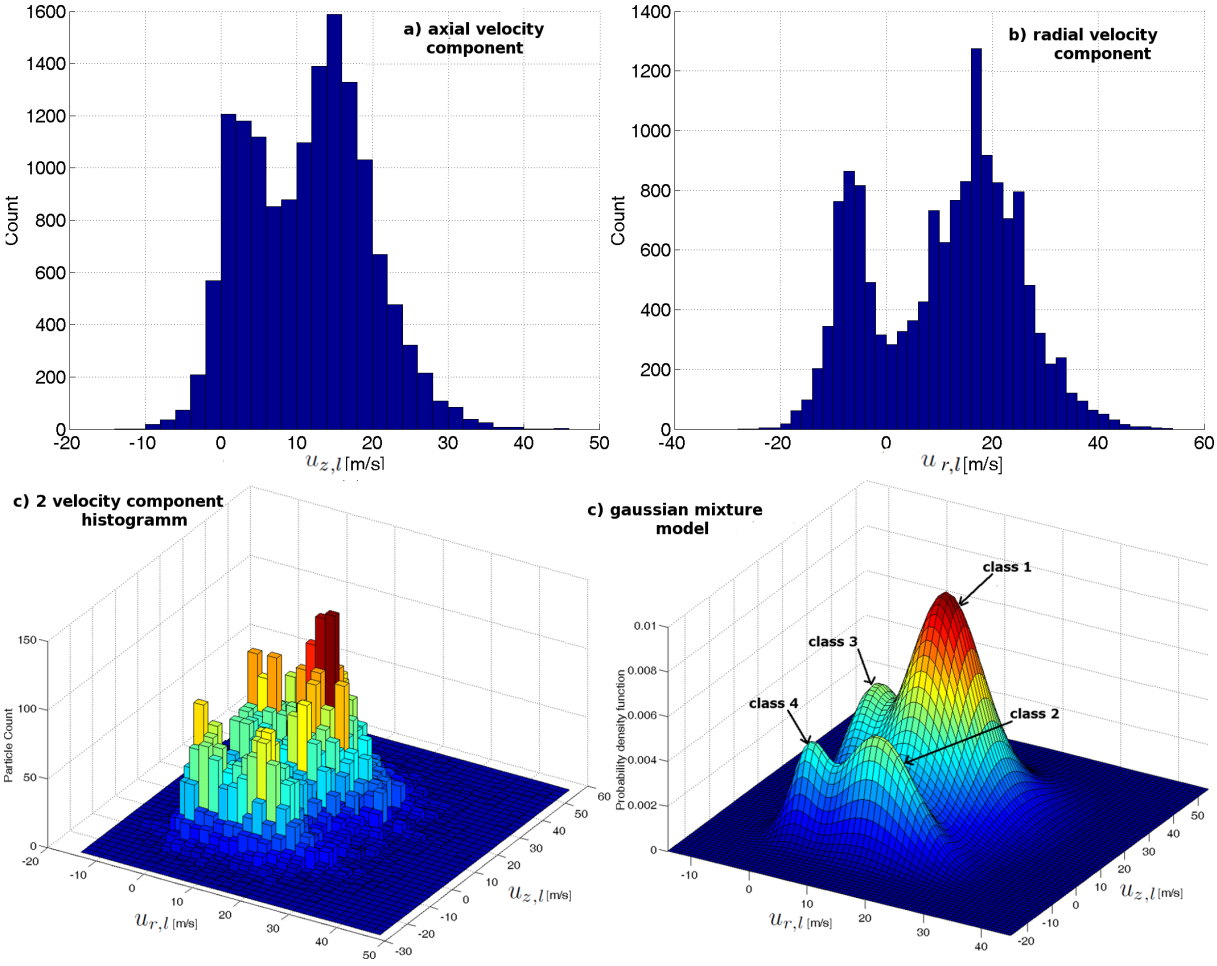

Figure 5. Mixture modelling analysis of velocity histogramms for OP2 (6 mm plane, R = 20 mm, vertical crossing).

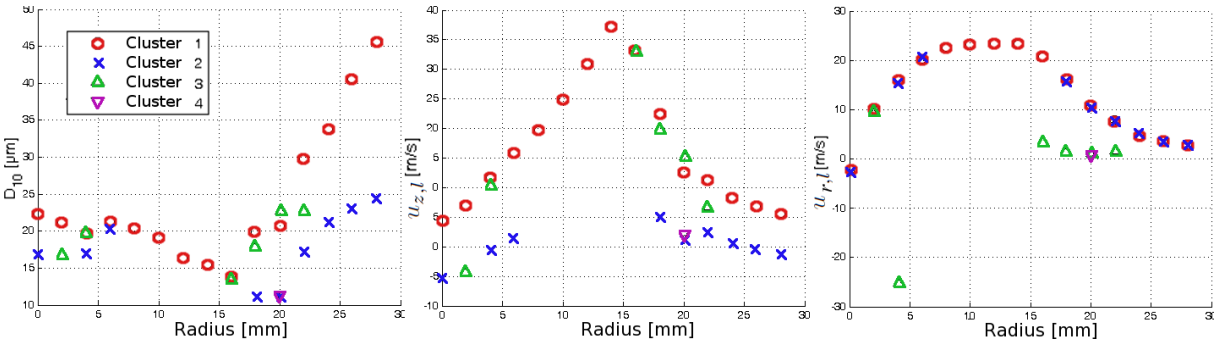

Figure 6. Synthesis of mixture modelling analysis of PDI data; $u_{z,l}$, $u_{r,l}$ and D_{10}; classes 2, 3 and 4 are identified as consequence of the recirculation.

Numerical simulation

Simulation of the two-phase flow field

Numerical simulation of the two phase flow is performed for the two operating points. For OP1, we validated the gas velocity field by comparing air flow simulation with LDA measurements. The simulation fits best the experimental data for the 56 mm plane, and keeps close for the other plane (*See* Fig. 7). For OP2, even if LDA data are not available, previous works on MERCATO showed that the gas velocity profiles for different air flows were similar. A comparison can be done using dimensionnless gas velocity. Comparison of the dimensionnless CFD velocity for OP2 with experimental data for OP1 shows equally good agreement.

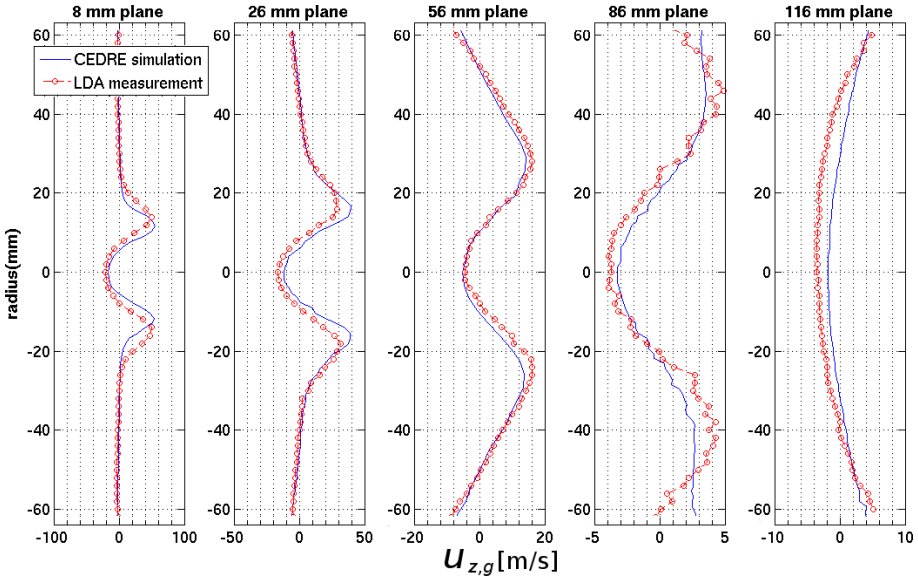

Figure 7. Comparison of RANS simulation and LDA measurement for OP1 ($u_{z,g}$)

Simulation of the liquid phase using lagrangian approach recquires to define injection points. For both cases, we modeled the injection section, located at 6 mm from the exit of the atomizer, by concentric circles. We assumed primary and secondary atomization phenomena already occured. The raw PDI data have been corrected, eliminating the recirculated particles. The distribution of the overall kerosene flow rate among the circle is reconstructed using the volume flow rate measured by PDI, which is proportional to the real volume flux.

Comparison of the PDI and CFD results remains good for the kerosene, especially for the velocity profile (*See* Fig.8). If we compare the dimensionless flow rate, the simulation reproduces well the distribution of the kerosene into the chamber (*See* Fig.9). We shall notice that the diameter profiles are less consistent with experimental data far from the injector plane (*See* Figs.10 and 11). The evaporation of droplets may be overestimated, because of the density of the spray near the injector, and of the modeling of the kerosene as a mono-component species. But CFD results remain quite good, and for OP2, the evaporation modeling shouldn't be an issue as we deal with ambient conditions.

Ignition results

Ignition model is tested for OP2, using 4 different spark plug positions located at {26;56;86;116} mm close to the wall. Experimental tests from Lecourt [11] have shown that ignition was not possible for the {86;116} mm positions. According to simulation, the local liquid equivalence ratio is lower for these positions than for the upstream ones (*See* Tab. 2). Concerning D_{10} and D_{32}, small differences were observed.

Kernel simulation duration is 0.5 ms. Near the wall, for the spark plug position, the RANS simulation gives $||\vec{u_g}|| \simeq 8m \cdot s^{-1}$, so the displacement of the kernel during the computation time would be around 12 mm, which is consistent with our vizualisation of the kernel.

The limit of the kernel is located by the maximum of the reaction rate $\dot{\omega}$ (*See* Fig. 12). At the beginning of each simulation, the front flame settles behind the limit of the initial energy deposit, then the radius increases. As criterion for gnition success or not, we use the evolution of $\dot{\omega}$ at the front flame. In the case of ignition success, the evolution curve shows a fast increase, if enough fuel vapour is produced.

For the {26;56} mm positions, $\dot{\omega}$ increase faster and higher than for the {86;116} mm cases, creating a bigger

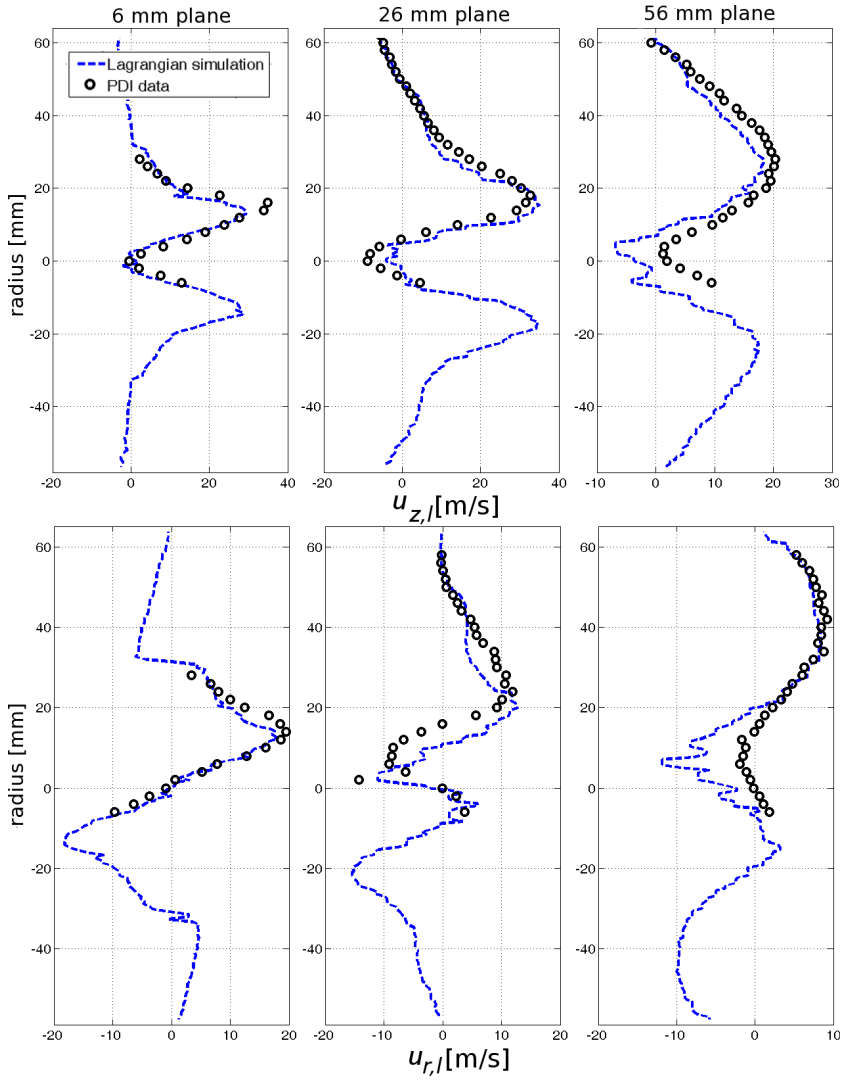

Figure 8. Comparison of lagrangian simulation to PDI measurement for OP1 (axial and radial velocity component)

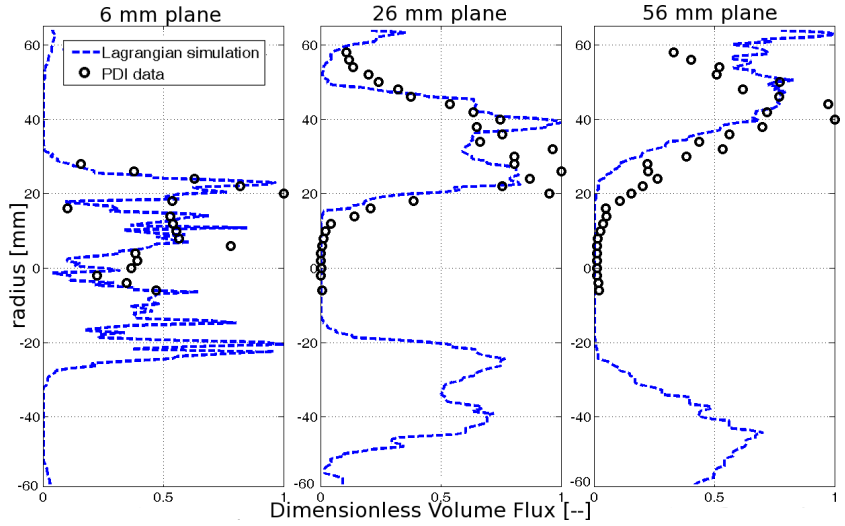

Figure 9. Comparison of lagrangian simulation to PDI measurement for OP1 (dimensionnless volume flux)

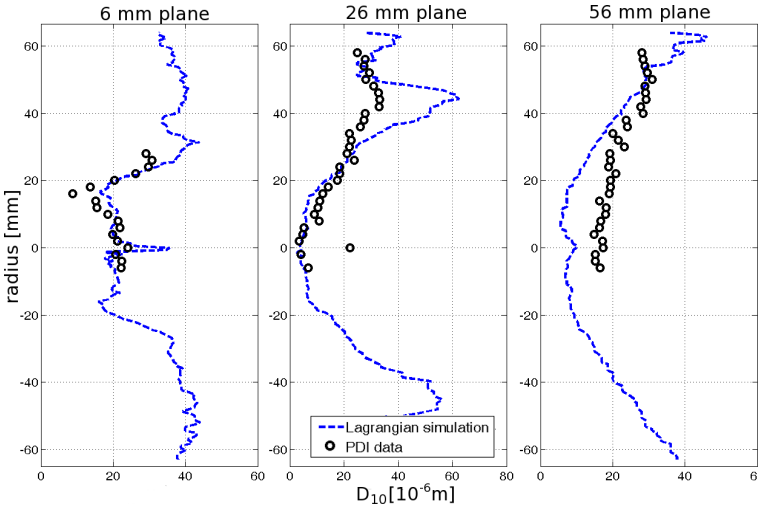

Figure 10. Comparison of lagrangian simulation to PDI measurement for OP1 (Arithmetic Diameter)

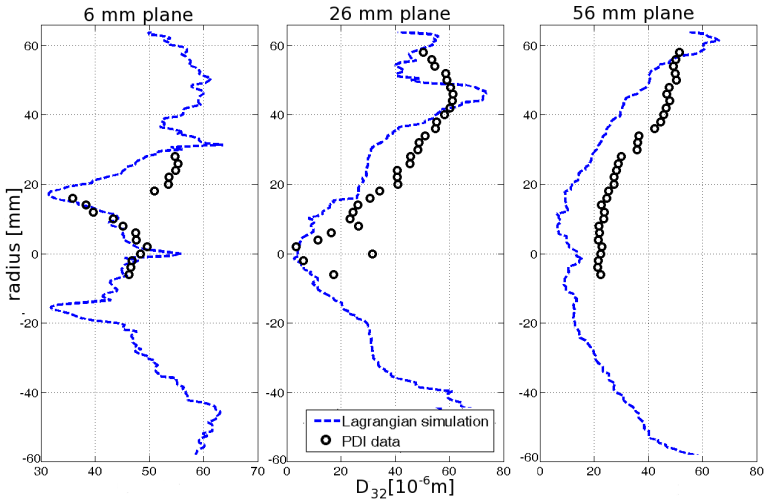

Figure 11. Comparison of lagrangian simulation to PDI measurement for OP1 (Sauter Mean Diameter)

Table 2. Experimental ignition tendencies for OP2 (x : success, o: failure) and computed liquid equivalence ratio among spark plug location

Plane (mm)	26	56	86	116
Ignition success	x	x	o	o
Φ_l	1.73	1.17	0.56	0.47

Plane (mm)	26	56	86	116
$D_{10}[\mu m]$	25.4	24.4	21.8	20.4
$D_{32}[\mu m]$	50.9	47.1	42.6	41.6

kernel. Then, the expansion speed of the kernel is quite the same for all cases. The difference of mean temperature between kernels is due to the energy consumed to evaporate droplets, more important for the position with higher equivalence ratio. At this point, it is not possible to predict the success or failure of ignition for these cases, even if we can notice different behaviours. The ignition possibility seems to be conditionned by global flow field rather than local parameters.

To complete our study, we tested the {26;56} mm position on the axis of the injector nozzle, inside the I.R.Z. For these cases, the local equivalence ratio is very low, and ignition is not possible at all, as we don't observe any

growth of $\dot{\omega}$ (*See* Fig. 13). Experimental study with laser ignition had been carried on MERCATO, and it was confirmed that ignition was not possible for these two positions.

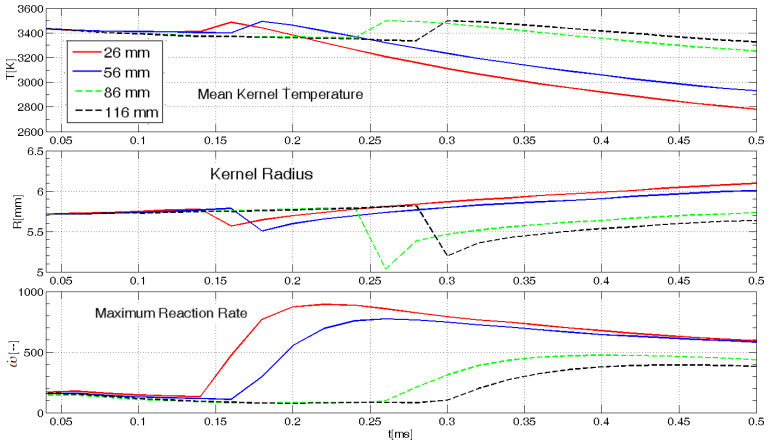

Figure 12. Kernel time evolution for the four spark plug positions, OP2 (dot line: experimental ignition failure)

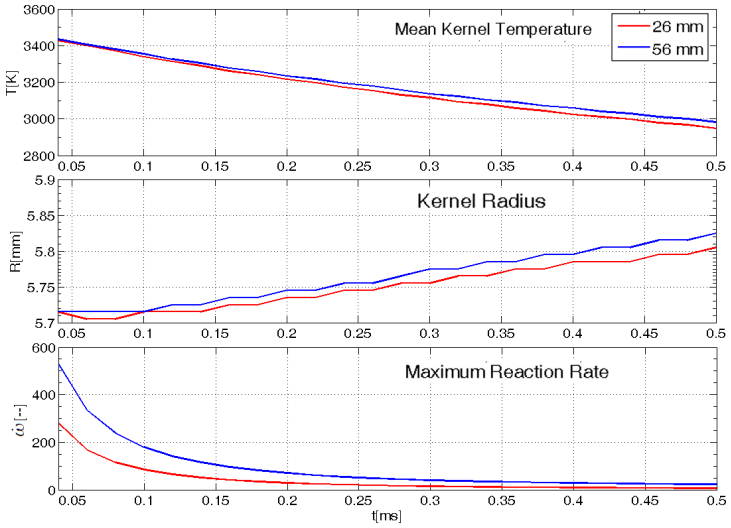

Figure 13. Kernel time evolution for an energy deposite on the chamber axis, OP2

Conclusions and perspectives

CFD simulations of the MERCATO combustor two-phase flow showed good agreement with the experimental data for non-reactive cases. The ONERA ignition model has been applied to one case, for several spark plug positions, with discriminant ignition tendencies. Differences have been observed between test cases. But sometimes, we have seen that the failure or success of ignition cannot be predicted with the use of the model alone. A complete simulation of ignition is to be done to eliminate doubts for position showing uncertain results with the model.

Nomenclature

LDA	Laser Doppler Anemometry
PDI	Phase Doppler Interferometry
CFD	Computational Fluid Dynamics
OP	Operating Point
C.R.Z	Corner Recirculation Zone
I.R.Z	Inner Recirculation Zone
D_{10}	Arithmetic mean diameter [m]
D_{32}	Sauter mean diameter [m]

Φ	Equivalence ratio
S_L	Flame Speed [m·s^{-1}]
α_s	Stoechiometric Fuel-Air-Ratio
Y	Mass fraction
T	Temperature [K]
u_z	Axial velocity component [m·s^{-1}]
u_θ	Tangential velocity component [m·s^{-1}]
u_r	Radial velocity component [m·s^{-1}]
ρ	Density [kg·m^{-3}]
$\dot{\rho}$	Mass source term [kg·m^{-3} ·s^{-1}]
$\bar{\rho}_l$	Partial liquid density [kg·s^{-3}]
$\dot{m}$	Mass flow [kg·s^{-1}]
λ	Thermal conductivity [W·m^{-1} ·K^{-1}]
c_p	Constant pressure heat capacity [J·K^{-1} ·kg^{-1}]
h	Mass enthalpy [J·kg^{-1}]
$\mathcal{D}$	Molar diffusion coefficient [m^2·s^{-1}]
$\mathcal{H}$	Enthalpy source term [J·kg^{-1} ·s^{-1}]
$\dot{\omega}$	Reaction rate [–]

Subscripts

g	Gas
l	Liquid
F	Fuel
χ	Relative to chemical reaction
v	Relative to evaporation phenomena
1	After spark discharge
2	At computational domain boundary
∞	Conditions far from the control volume

Acknowledgements

The authors would like to acknowledge the financial support and contribution from Turbomeca.

References

[1] Widmann, J.R., and Presse, C., *Combustion and Flame* 129:47-86 (2002).
[2] Ikeda, Y., Yamada, N., and Mandai, S., *Proceedings of the Combustion Institute* 29:853-859 (2002).
[3] Read, R.W., Rogerson, J.W., and Hochgreb, S. *46th AIAA Aerospace Sciences Meeting and Exhibit* (2008).
[4] Marchione, T., Ahmed, S.F., and Mastorakos, E., *Combustion and Flame* 156:166-185 (2009).
[5] Quintilla, V., "Étude du rallumage à haute altitude des chambres de combustion de turboréacteurs" , *PhD thesis, Université de Toulouse* (2002).
[6] Ouarti, N., "Modélisation de l'allumage d'un brouillard de carburant dans un foyer de turbomachine", *PhD thesis, Université de Toulouse* (2004).
[7] García Rosa, N., "Phénomènes d'allumage d'un foyer de turbomachine en conditions de haute altitude",*PhD thesis, Université de Toulouse* (2008).
[8] García Rosa, N., Linassier, G., Lecourt, R., Villedieu, P., and Lavergne, G., *Sixth International Symposium on Multiphase Flow, Heat Mass Trnasfer and Energy Conversion*, Xi'an, China, July 2009, Paper No. FG-27.
[9] Westbrook, C.K., and Dryer, F.L., *Combustion Science and Technology* 27:31-43 (1981).
[10] Biernacki, C., Celeux, G., and Langrognet, F., *Computationnal Statistics and Data Analysis* 51/2:587-600 (2006).
[11] Lecourt,"Ignition and Extinction results at ambient conditions," Timecop Report No. D2.2.1a.
[12] Chrigui, M., Janicki, A. and Janicka, J., *Atomization and spray* 19(10):929-955 (2009).
[13] Lecourt,"Injection system two-phase flow characterization (LDA-PDA)," Timecop Report No. D2.2.1c.